Phosphorylation of the Plasma Membrane Calcium Pump at High ATP Concentration. On the Mechanism of ATP Hydrolysis†

María M. Echarte, Rolando C. Rossi,* and Juan Pablo F. C. Rossi*

Departamento de Química Biológica, IQUIFIB, Facultad de Farmacia y Bioquímica, Universidad de Buenos Aires, Junín 956, 1113 Buenos Aires, Argentina

Received September 6, 2006; Revised Manuscript Received November 15, 2006

ABSTRACT: The plasma membrane calcium ATPase (PMCA) reacts with ATP to form acid-stable phosphorylated intermediates (*E*P) that can be measured using (γ-^{32}P)ATP. However, the steady-state level of *E*P at [ATP] higher than 100 μM has not yet been studied due to methodological problems. Using a microscale method and a purified preparation of PMCA from human red blood cells, we measured the steady-state concentration of *E*P as a function of [ATP] up to 2 mM at different concentrations of Mg^{2+}, both at 4 and 25 °C. We have measured the Ca^{2+}-ATPase activity (v) under the same conditions as those used for phosphorylation experiments. While the curves of ATPase activity vs [ATP] were well described by the Michaelis−Menten equation, the corresponding curves of *E*P required more complex fitting equations, exhibiting at least a high- and a low-affinity component. Mg^{2+} increases the apparent affinity for ATP of this latter component, but it shows no significant effect on its high-affinity one or on the Ca^{2+}-ATPase activity. We calculated the turnover of *E*P (k_{pEP}) as the ratio v/*E*P. At 1 mM Mg^{2+}, k_{pEP} increases hyperbolically with [ATP], while at 8 μM Mg^{2+}, it exhibits a behavior that cannot be explained by the currently accepted mechanism for ATP hydrolysis. These results, together with measurements of the rate of dephosphorylation at 4 °C, suggest that ATP is acting in additional steps involving the interconversion of phosphorylated intermediates during the hydrolysis of the nucleotide.

P-type ATPases are a group of enzymes responsible for active transport of cations across the cell membrane, using the hydrolysis of ATP as a source of energy. During the reaction cycle they form phosphorylated intermediates, *E*P,[1] whose concentration can be measured by stopping the reactions by denaturation in acid media.

The plasma membrane calcium pump (PMCA) is a P-type ATPase whose abundance is approximately 0.01% of the total proteins present in the membrane (*1*). Combining the knowledge on the elementary steps and steady-state kinetics of the Ca^{2+}-ATPase with what was known from other cation transport ATPases, Rega and Garrahan postulated the kinetic model represented in Scheme 1 (*2*).

The model proposes that the enzyme exists in two main conformations, E_1 and E_2. Upon binding of ATP and Ca^{2+}, E_1 can be phosphorylated, leading to the formation of the intermediates E_1P and E_2P. It is generally accepted that Ca^{2+} would be transported after binding to cytoplasmic sites in E_1 and released from the E_2P intermediate at extracellular sites.

Scheme 1

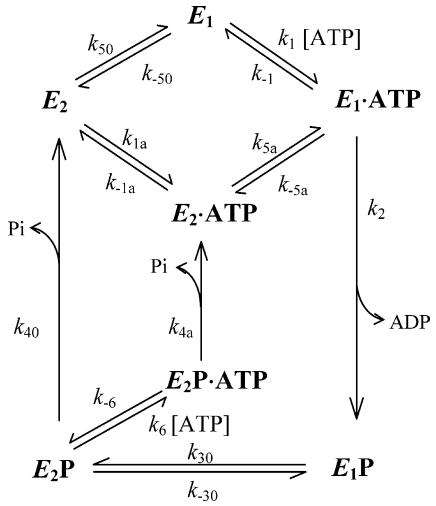

According to Scheme 1, ATP would be involved in three different steps of the reaction cycle: phosphorylation, dephosphorylation, and $E_2 \rightarrow E_1$ transition. These authors found two kinds of sites for ATP binding: one of high affinity ($K_m \approx 2.5$ μM) and catalytic activity and another one of low affinity ($K_m \approx 140$ μM) that would be an activating site (*2*, *3*). Besides its role as a cofactor of ATP as the substrate of the ATPase, Mg^{2+} has been shown to participate as an activator not only of the phosphorylation but also of the dephosphorylation reaction and of the conformational transitions of both phosphorylated and dephosphorylated forms (*2*, *4*−*7*).

† This work was supported by Consejo Nacional de Investigaciones Científicas y Técnicas (CONICET), Universidad de Buenos Aires, Agencia Nacional de Promoción Científica y Tecnológica, and the National Institutes of Health, FIRCA Grant 1 R03 TW006837-01A1. R.C.R. and J.P.F.C.R. are established investigators of CONICET.

* To whom correspondence should be addressed. Tel: (+5411) 4 964 5506. Fax: (+5411) 4 962 5457. E-mail: jprossi@mail.retina.ar; rcr@mail.retina.ar.

[1] Abbreviations: $C_{12}E_{10}$, polyoxyethylene 10-lauryl ether; DTT, dithiothreitol; EGTA, ethylene glycol bis(β-aminoethyl ether)-*N*,*N*,*N*′,*N*′-tetraacetic acid; *E*P, phosphorylated enzyme; MOPS, 3-(*N*-morpholino)-propanesulfonic acid; PMCA, plasma membrane calcium ATPase.

10.1021/bi061857x CCC: $37.00
Published on Web 01/06/2007

Formation of *E*P (which includes E_1P and E_2P forms) has been demonstrated using electrophoretic techniques (*8*−*10*) and quantified using filtration or centrifugation methods (*10*−*14*). Because of the high level of blanks and/or scatter, typical procedures to measure *E*P of the PMCA are limited to ATP concentrations lower than 100 μM (*14*), i.e., far below physiological intracellular concentrations of the nucleotide (*15*). This limitation becomes more important if only small amounts of protein are available. In order to study the behavior of PMCA phosphoenzyme at higher ATP concentrations, we have developed a procedure that combines a microscale electrophoretic technique with computer-assisted image analysis (*16*).

The purpose of this work was to extend the study of the effect of ATP and Mg^{2+} on the activity and *E*P level of the PMCA to physiological concentrations of these ligands to gain further insight into the PMCA reaction mechanism. We first performed experiments at low temperature (0−4 °C) in order to slow the rates of the reactions, thus facilitating the measurements. These experiments included measurements of activity and phosphoenzyme levels in the steady state, which were also carried out at 25 °C in order to investigate the validity of the conclusions obtained at low temperature. Results in this paper show that ATP is involved in the pathway of *E*P formation and breakdown in a manner that is not adequately explained by the currently accepted mechanism.

EXPERIMENTAL PROCEDURES

All of the chemicals used in this work were of analytical grade and were primarily purchased from Sigma Chemical Co. Freshly drawn human blood was obtained from the Hematology Section of the Hospital de Clínicas General José de San Martín, Argentina. (γ-^{32}P)ATP was obtained from Dupont NEN. Kodak X-OMAT film was obtained from Sigma Chemical Co.

Purification of the Ca^{2+} Pump from Human Erythrocytes. Calmodulin-depleted erythrocyte membranes were prepared as described previously (*17*, *18*). Ca^{2+}-ATPase was isolated in pure form by calmodulin affinity chromatography (*19*) in the presence of asolectin and $C_{12}E_{10}$; homogeneity was verified by SDS−PAGE (single band at M_r 138000). Prior to use, the enzyme was kept in storage buffer (0.2 mg/mL asolectin, 0.5 mg/mL $C_{12}E_{10}$, 300 mM KCl, 10 mM MOPS−K, pH 7.4 at 4 °C, 2 mM EGTA, 2 mM $CaCl_2$, and 2 mM DTT) under liquid nitrogen. The most active fraction eluted from the column was used for the experiments (about 2 mL in a typical preparation). The protein concentration in this fraction was around 90 μg/mL, and its activity was 309 ± 32 μmol of ATP hydrolyzed (mg of protein)$^{-1}$ h^{-1}. Protein concentrations were measured according to Peterson (*20*).

Free Ca^{2+} and Mg^{2+}. The concentration of free Ca^{2+} was measured using a specific electrode (93-20, Orion Research, Inc.) as described by Kratje et al. (*21*). Free Mg^{2+} was calculated by measuring the displacement of Ca^{2+} from its complexes with ATP and EGTA in media of the same composition as those used to measure ATPase activity and phosphoenzyme concentration. The concentrations of Mg^{2+} and Ca^{2+} given in the figures are those of the free cations.

Determination of Contaminant Mg^{2+}. The concentration of Mg^{2+} present in the incubation media in the absence of added $MgCl_2$ was determined as described by Caride et al. (*7*), taking advantage of the fact that Mg^{2+} is an essential activator of the Na^+/K^+-ATPase. The contaminant (free) Mg^{2+} concentration was found to be 8 μM.

Measurement of the Ca^{2+}-ATPase Activity. ATPase activity was measured in a medium containing 30 mM Tris-HCl, pH 7.4, 2 mM EGTA, enough calcium to reach 100 μM (free) Ca^{2+}, 150 mM KCl, 0.5 mg/mL asolectin, 0.5 mg/mL $C_{12}E_{10}$, and the concentrations of ATP and Mg^{2+} indicated in the figures. Ca^{2+}-ATPase activity was measured as the difference between the activity in the aforementioned medium and that in the same medium without Ca^{2+}, i.e., in the presence of 2 mM EGTA. The protein concentration ranged from 2 to 5 μg/mL purified enzyme. Release of P_i from (γ-^{32}P)ATP was estimated according to the procedure of Richards et al. (*3*).

Phosphorylation Procedure. Purified PMCA (4 μg) was phosphorylated as described by Echarte et al. (*16*). Enzyme phosphorylation was carried out in a medium containing 30 mM Tris-HCl (pH 7.4 at 4 °C), 2 mM EGTA, enough calcium to reach 100 μM (free) Ca^{2+}, 150 mM KCl, 0.5 mg/mL asolectin, 0.5 mg/mL $C_{12}E_{10}$, and the different reagents described in the legend to the figures. The reaction was started by the addition of (γ-^{32}P)ATP under vigorous stirring and, after 3 min, was stopped with an ice-cold solution of TCA (7% w/v final concentration).

Dephosphorylation Procedure. After the steady state was reached, phosphorylation was stopped by the addition of 2 mM EGTA and enough asolectin, $C_{12}E_{10}$, ATP, and Mg^{2+} to maintain the phosphorylation conditions. Dephosphorylation was allowed to proceed during the time periods described in the figures and stopped by adding TCA (10% w/v). For these experiments we used a thermostated rapid mixing apparatus, SFM-4 from Bio-Logic (France), as described by Schwarzbaum et al. (*22*). The reaction mixture was received in a conical tube and analyzed for *E*P (*16*).

Isolation of EP by SDS−PAGE. After the phosphorylation reaction was stopped, the tubes were spun down at 7000 rpm for 3.5 min at 4 °C. The samples were then washed once with 7% TCA, 50 mM H_3PO_4, and 0.5 mM ATP and once with double distilled water and processed for SDS−PAGE. For this purpose, the pellets were dissolved in a medium containing 150 mM Tris-HCl (pH 6.5 at 14 °C), 5% SDS, 5% DTT, 10% glycerol, and bromophenol blue (sample buffer). Electrophoresis was performed at pH 6.3 (14 °C) in a 4−20% continuous gradient 1 mm thick slab gel. The reservoir buffer was 0.1 M sodium phosphate, pH 6.3, with 0.1% SDS. Migration of the sample components took place at 14 °C, with a current of 60 mA until the tracking dye reached a distance of about 10 cm from the top of the gel. Gels were stained, dried, and exposed to a X-OMAT film (Kodak) at −70 °C as detailed in Echarte et al. (*16*).

Densitometric Analysis. Unsaturated autoradiograms and stained gels were scanned with a Umax Vista S12 scanner. Analysis of the images was performed with Sigmagel gel analysis software (SPSS Inc.). *E*P quantification was achieved as described in Echarte et al. (*16*).

Data Analysis. Experiments presented in Results were representative of at least four independent experiments. Theoretical equations were adjusted to the results by nonlinear regression based on the Gauss−Newton algorithm using commercial programs (Excel and Sigma-Plot for

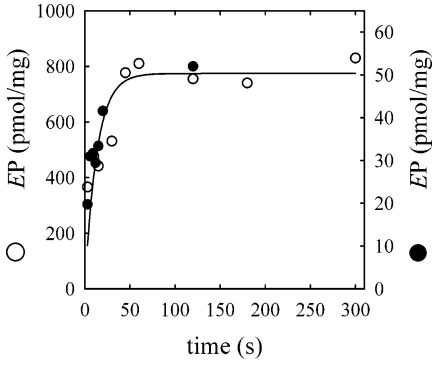

FIGURE 1: Time course of phosphorylation. Phosphorylation of purified PMCA was carried out at 4 °C in the presence of 8 μM Mg^{2+} and 10 μM (●) or 1 mM (○) ATP. The continuous line is a single increasing exponential function of time with a rate coefficient k equal to 0.08 s^{-1}.

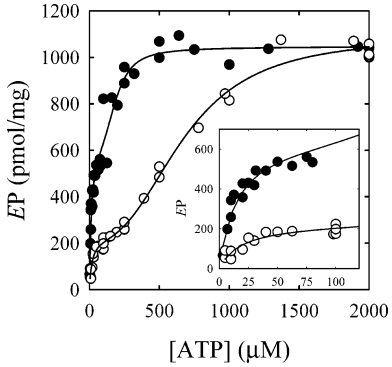

FIGURE 2: Steady-state level of *E*P as a function of [ATP]. Phosphorylation of purified PMCA was carried out at 4 °C in the presence of 8 μM (○) or 1 mM (●) Mg^{2+}. The continuous line represents the fitting of the empirical eq 2 to the experimental data with the best fitting parameter values detailed in Table 1. Inset: *E*P vs [ATP] up to 100 μM. The data represent results of seven independent experiments.

Windows). To choose among different equations, we applied the second-order Akaike information criterion, that is

$$\mathrm{AIC} = N \ln(S) + 2P \qquad (1)$$

where N is the number of data, S is the sum of weighted square errors of residuals, and P is the number of parameters of the fitted function (*23*). We chose the equations that gave the lower value of AIC. Parameter values are given as their mean ± standard error. To solve the equations of the reaction mechanism, we used Mathematica for Windows.

RESULTS AND DISCUSSION

EP Dependence on ATP Concentration at 4 °C. In order to determine the time at which the steady state was reached covering a wide range of [ATP], we measured the concentration of phosphoenzyme *E*P as a function of time in media with 10 μM or 1 mM ATP and 8 μM Mg^{2+}. Results, which are shown in Figure 1, can be described by single exponential curves with *E*P (steady state) = 51 ± 3 pmol/mg and rate coefficient $k = 0.1 \pm 0.01$ s^{-1} at 10 μM ATP and *E*P (steady state) = 775 ± 53 pmol/mg and $k = 0.08 \pm 0.02$ s^{-1} at 1 mM ATP.

Figure 2 shows the steady-state level of *E*P vs [ATP] from 5 to 2000 μM measured in the presence of 8 μM and 1 mM Mg^{2+}. The curves display a complex behavior that can be empirically described by the sum of two components, a hyperbolic one of high affinity for ATP and a sigmoid one of lower affinity for the nucleotide. The continuous lines in Figure 2 are plots of the empirical equation:

$$E\mathrm{P} = \frac{E\mathrm{P}_{\max 1}[\mathrm{ATP}]}{K_{\mathrm{m}1} + [\mathrm{ATP}]} + \frac{E\mathrm{P}_{\max 2}[\mathrm{ATP}]^n}{K_{\mathrm{m}2}{}^n + [\mathrm{ATP}]^n} \qquad (2)$$

where $E\mathrm{P}_{\max 1}$ and $E\mathrm{P}_{\max 2}$ are the maximal levels and $K_{\mathrm{m}1}$ and $K_{\mathrm{m}2}$ are apparent dissociation constants for ATP of the high- and low-affinity components of *E*P, respectively, and n is a coefficient that measures the degree of sigmoidicity of the second component. Values of the best fitting parameters are shown in Table 1. It is clear that while the *E*P level at [ATP] tending to infinity, i.e., $E\mathrm{P}_{\max 1} + E\mathrm{P}_{\max 2}$, remains almost unchanged with [Mg^{2+}], the value of $E\mathrm{P}_{\max 1}$ increases (see inset) at the expense of that of $E\mathrm{P}_{\max 2}$. Increasing [Mg^{2+}] produces a 4-fold increase in the affinity for ATP of the sigmoid component. When working at low [ATP], we observe that ATP affinity is not modified by Mg^{2+}, and its value is in agreement with others previously reported (*3*, *24*). The value of n was set at 1, 2, or 3 or was freely fitted to the data. Table 1 shows that, according to the AIC criterion, $n = 3$ gave best fit for 8 μM Mg^{2+} and that, at 1 mM Mg^{2+}, values of 2 and 3 were equally good, while when n was adjusted, values of n were between 2 and 3 for both [Mg^{2+}].

Using $n = 2$, eq 2 can be rearranged to a rational function containing terms in [ATP] up to third degree, which indicates that binding of ATP occurs at least in three different steps of the reaction cycle (*25*). It is important to note that for any steady-state property of an enzyme, as it is for the measurement of *E*P, this does not mean that the enzyme actually possesses three different coexisting sites. Solving the equations for the currently accepted mechanism (Scheme 1) yields a rational function of third degree that would be compatible with the data obtained. When working at 8 μM Mg^{2+}, a value of $n = 3$ suggests that ATP would be involved in at least four different steps of the reaction cycle. This is an indication that the proposed mechanism does not explain the dependence of *E*P on [ATP] when working at limiting Mg^{2+} concentrations.

Dependence of Ca^{2+}-ATPase Activity on the Concentration of ATP at 4 °C. In order to study how the dependence of *E*P on [ATP] would be reflected on the overall pump activity, we determined the velocity of ATP hydrolysis under the same conditions as those used to measure the formation of *E*P. Figure 3 shows the Ca^{2+}-ATPase activity vs [ATP] curve for purified enzyme in the presence of 8 μM or 1 mM Mg^{2+}. In both cases, activity follows Michaelis−Menten kinetics, which is characteristic of the calmodulin-free enzyme (*26*−*28*). Although $V_{\max}$ increases from 0.87 ± 0.03 μmol (mg of protein)$^{-1}$ h^{-1} to 3.7 ± 0.2 μmol (mg of protein)$^{-1}$ h^{-1} when [Mg^{2+}] is varied from 8 μM to 1 mM, K_{m} shows only a slight change, from 34.2 ± 5.8 μM to 53 ± 10 μM, in agreement with previous results (*3*). These values of K_{m} lay between those reported for the high- and low-affinity ATP sites of the PMCA in the presence of calmodulin (*26*, *29*).

The Michaelis−Menten behavior observed for the results in Figure 3, which contrasts with the more complex shape of the *E*P vs ATP curves in Figure 2, could imply that some of the reactions that depend on the concentration of ATP and that are involved in the formation and breakdown of

Table 1: Best Fitting Values of the Parameters of Eq 2 Adjusted to the Data in Figure 2 at 8 μM or 1 mM Mg^{2+}

parameter	value ± 1 SE at 8 μM Mg^{2+}				value ± 1 SE at 1 mM Mg^{2+}			
n	2.6 ± 0.3	3[a]	2[a]	1[a]	2.5 ± 1.0	3[a]	2[a]	1[a]
K_{m1} (μM)	12.5 ± 4.5	17.8 ± 6.3	6.1 ± 3.3	1.1 ± 4.2	6.7 ± 5.9	5.9 ± 4.2	4.4 ± 4.1	5.3 ± 5.5
EP_{max1} (pmol/mg)	223 ± 22	248 ± 24	178 ± 22	79 ± 3	548 ± 132	560 ± 70	485 ± 88	367 ± 172
K_{m2} (μM)	687 ± 49	692 ± 38	708 ± 76	1453 ± 329	162 ± 34	174 ± 26	149 ± 29	145 ± 81
EP_{max2} (pmol/mg)	877 ± 75	828 ± 62	995 ± 104	1703 ± 156	501 ± 143	445 ± 68	572 ± 83	793 ± 143
AIC	461	460	463	514	282	281	281	290

[a] These values of n were fixed during the fitting analysis.

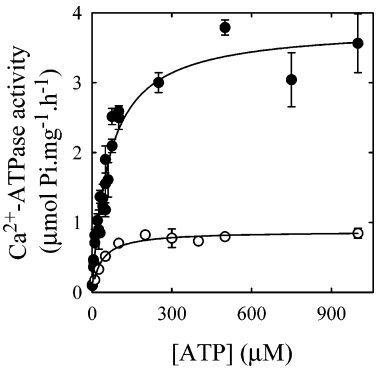

FIGURE 3: Ca^{2+}-ATPase activity as a function of [ATP]. PMCA Ca^{2+}-ATPase activity was measured in the same conditions as those used to measure EP in the presence of 8 μM (○) and 1 mM (●) Mg^{2+} at 4 °C. The continuous line represents the fitting of a Michaelis−Menten equation to the experimental data. Error bars represent the standard deviation of the data ($n = 3$).

Scheme 2

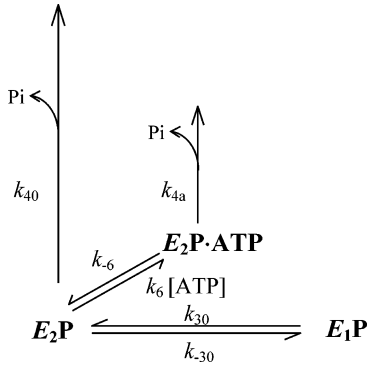

the EP intermediates do not have a significant effect on the rate of ATP hydrolysis. As a first approach to address this point, we analyzed the ratio between the activity and the steady-state level of EP.

Dependence of the Turnover of EP on [ATP] at 4 °C. The lower left part of the model in Scheme 1 (Scheme 2) describes the reactions in which EP species are involved. In steady-state conditions, the rate of ATP hydrolysis can be expressed as

$$v = [E_2P]k_{40} + [E_2P{\cdot}ATP]k_{4a} = [E_1P]k_3 - [E_2P]k_{-3} \quad (3)$$

and the rate of dephosphorylation via k_{4a} should equal the net rate of binding/ dissociation of ATP to E_2P, i.e.

$$[E_2P{\cdot}ATP]k_{4a} = [E_2P]k_6[ATP] - [E_2P{\cdot}ATP]k_{-6} \quad (4)$$

Considering the total concentration of EP:

$$[EP] = [E_1P] + [E_2P] + [E_2P{\cdot}ATP] \quad (5)$$

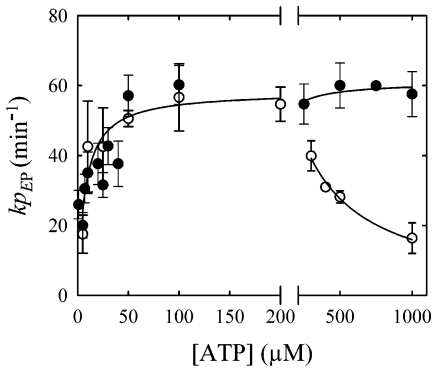

FIGURE 4: k_{pEP} as a function of [ATP]. Turnover of the phosphorylated intermediates of the erythrocyte PMCA was calculated as the ratio between Ca^{2+}-ATPase activity (Figure 3) and EP (Figure 2) in the presence of 8 μM (○) and 1 mM (●) Mg^{2+}. Values obtained were plotted as a function of ATP. The continuous line represents the fitting of eq 6 to the experimental data up to 200 μM. For higher concentrations of ATP these were drawn by eye.

the ratio between v and [EP], which is formally equal to the turnover of EP (k_{pEP}), can be calculated as

$$\frac{v}{[EP]} = k_{pEP} = \frac{k_{pEP_0}K_{ATP} + k_{pEP\infty}[ATP]}{K_{ATP} + [ATP]} \quad (6)$$

where

$$k_{pEP_0} = \frac{k_3k_{40}}{k_3 + k_{-3} + k_{40}} \quad (7)$$

$$k_{pEP\infty} = \frac{k_3k_{4a}}{k_3 + k_{4a}} \quad (8)$$

and

$$K_{ATP} = \frac{(k_{-6} + k_{4a})(k_3 + k_{-3} + k_{40})}{k_6\,(k_3 + k_{4a})} \quad (9)$$

Equation 6 predicts that as [ATP] increases from zero to infinity, the turnover of EP should vary from k_{pEP_0} to $k_{pEP\infty}$ along a hyperbola with $K_{0.5}$ equal to K_{ATP}. An additional advantage of this treatment is that the number of rate constants to be analyzed is reduced to that appearing in Scheme 2.

In Figure 4 we plotted k_{pEP} as a function of the concentration of ATP. At 1 mM [Mg^{2+}], k_{pEP} increases with [ATP] following a rectangular hyperbola (as predicted by eq 6). In contrast, when 8 μM Mg^{2+} is present, k_{pEP} first grows, reaches a maximum at 100−200 μM ATP, and then drops significantly at higher concentrations of the nucleotide. It is noticeable that for ATP concentrations below 200 μM there

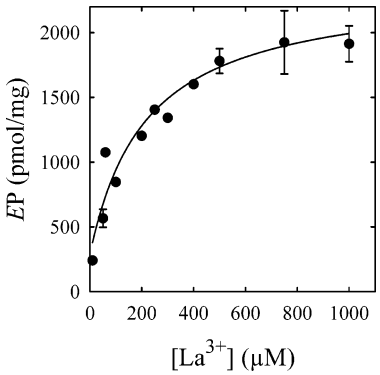

FIGURE 5: *E*P dependence on La^{3+} concentration. Phosphorylation of purified PMCA was carried out in the presence of 50 μM (γ-^{32}P)ATP and different [La^{3+}]. Error bars represent the standard deviation of the data ($n = 4$). The continuous line represents the fitting of a Michaelis−Menten-like equation plus a constant term (for parameter values see the main text).

are no significant differences between k_{pEP} at 8 μM and 1 mM Mg^{2+}. For this range of concentrations of ATP, continuous lines in Figure 4 represent the solution of eq 6 for its best fitting values: $k_{pEP_0} = 18 \pm 4$ min^{-1}, $k_{pEP\infty} = 63 \pm 4$ min^{-1}, and $K_{ATP} = 27 \pm 10$ μM.

The behavior of k_{pEP} observed at 1 mM Mg^{2+} would indicate that ATP accelerates the dephosphorylation of the enzyme with high apparent affinity and is consistent with the model proposed by Rega and Garrahan (see page 115 in ref *2*). A similar behavior has been previously reported for the Na,K-ATPase (*22*), although the authors found that ATP does not accelerate dephosphorylation, but they rather postulate that the rate of the $E_1P \rightarrow E_2P$ transition is affected. On the contrary, when 8 μM Mg^{2+} is present, results show a more complex behavior and suggest that, in addition to those shown in Scheme 2, other reactions connecting the phosphorylated forms should be affected by the concentration of ATP. The fact that at sufficiently high Mg^{2+} concentration this complex behavior is not observed would indicate that Mg^{2+} is driving the pathway to that of Scheme 2.

How Much Enzyme Can Be Phosphorylated? For the PMCA, the amount of *E*P obtained in the presence of lanthanum is usually considered as a valid calculation of the total active enzyme concentration (*30*−*32*). It has been proposed that La^{3+} would act as a dead-end inhibitor capable to bring the entire amount of functionally active enzyme into the E_1P form. If this were the case, and considering a molecular weight of the PMCA of 138000, it is expected a total of 7250 pmol of *E*P/mg of enzyme. Results of the measurement of *E*P in our purified preparation as a function of [La^{3+}] and in the presence of 50 μM ATP are shown in Figure 5. Analysis of the data by nonlinear regression, fitting a Michaelis−Menten-like equation plus a constant term, gives a maximum concentration of 2270 ± 224 pmol of *E*P/mg of protein and $K_{0.5}$ for La^{3+} of 191 ± 81 μM, with an *E*P concentration in the absence of La^{3+} of 233 ± 163 pmol of *E*P/mg of protein. Using the classical filtration method, Kosk-Kosicka et al. (*14*) reported a maximum of 2400 pmol of *E*P/mg of PMCA. This large difference with the predicted value given above could be due to the presence of proteins other than PMCA and/or to inactivation of the enzyme during its purification process, as proposed for SERCA (*33*) and for Na^+/K^+-ATPase (*34*). However, given the high level of PMCA purity detected in the SDS−PAGE gels and the mildness of the detergent used to purify the enzyme used in our studies, these possibilities seem unlikely, and other alternatives should be examined (see Concluding Remarks below).

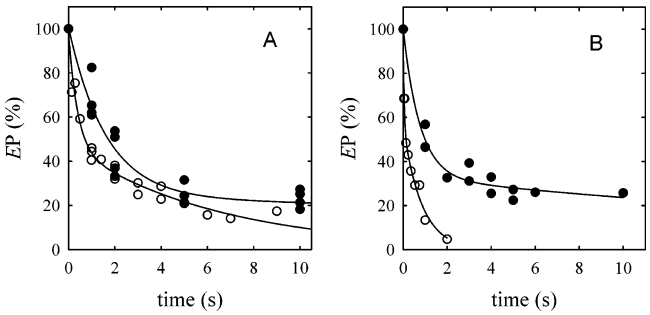

FIGURE 6: Time course of dephosphorylation of PMCA. Phosphorylation of purified PMCA was carried out at 4 °C in the presence of 10 μM (●) or 1 mM (○) (γ-^{32}P)ATP and 8 μM (A) or 1 mM (B) Mg^{2+}. After 3 min incubation, the reaction was stopped by adding a 2 mM EGTA solution. Dephosphorylation was allowed to proceed during the time lapse detailed in each figure and then stopped by protein precipitation with TCA (7%). Results are plotted as the percent of their initial values, which were (in pmol/mg of protein) (A) 51.3 at 10 μM ATP, 814 at 1 mM ATP and (B) 342 at 10 μM ATP, 968 at 1 mM ATP. Continuous lines represent the fitting of eq 10 to the experimental data with best fitting parameters detailed in Table 2.

According to our results in Figures 2 and 5, *E*P in the steady state represents a maximum of about 50% of the total active enzyme at saturating ATP concentrations.

PMCA Dephosphorylation at 4 °C. As we discussed above, k_{pEP} depends on the rates of both *E*P dephosphorylation and $E_1P \leftrightarrow E_2P$ transition. In order to discriminate which of these steps are modified by ATP and hence modify k_{pEP}, we measured the time course of (γ-^{32}P)*E*P decay after addition of EGTA to the enzyme performing steady-state ATPase activity.

Garrahan and Rega (*35*) showed that ATP accelerates dephosphorylation only when the phosphoenzyme was formed in the presence of Mg^{2+}. Herscher et al. (*5*) obtained values for dephosphorylation constants and studied the effect of ATP when phosphoenzyme was formed in the presence of low [ATP].

In this work, we measured the dephosphorylation rate once phosphorylation has been carried out in the presence of both low and physiological ATP concentrations. The effect of Mg^{2+} in this process has been investigated as well. Figure 6 shows *E*P decay measured in the presence of 10 μM (panel A) or 1 mM (panel B) ATP and 8 μM or 1 mM Mg^{2+}. As shown by Herscher et al. (*5*), *E*P decays in a biphasic way. We fitted the following equation to the experimental data:

$$EP = EP_f e^{-k_f t} + EP_s e^{-k_s t} \qquad (10)$$

where EP_f and EP_s are the amplitudes and k_f and k_s are the apparent rate constants of the fast and slow *E*P decay components, respectively. The best fitting parameters for this equation are detailed in Table 2.

It can be seen that ATP increases the dephosphorylation rate in the presence of both limiting and nonlimiting Mg^{2+} concentrations. These results agree with those found by Muallem and Karlish (*27*) but only partially with those reported by Rega and Garrahan (*36*), who observed that ATP had no effect on the dephosphorylation rate in the absence

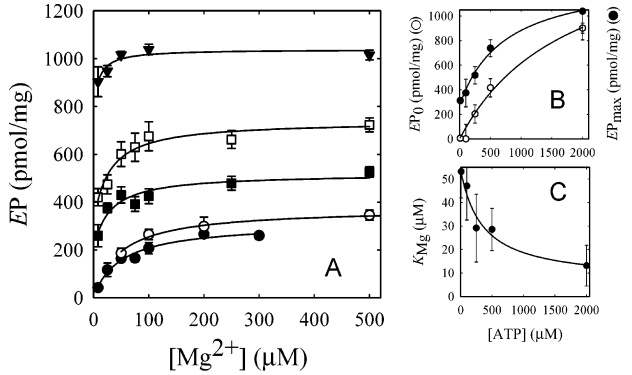

FIGURE 7: Steady-state level of *E*P as a function of [ATP] and [Mg^{2+}]. Phosphorylation of purified PMCA was carried out at 4 °C in the presence of 8−500 μM Mg^{2+} and with 10 (●), 100 (○), 250 (■), 500 (□), and 2000 (▼) μM ATP, respectively. The *E*P steady-state level was plotted as a function of Mg^{2+} for each [ATP] assayed (panel A). Continuous lines represent the fitting of eq 12 to the experimental data. Panels B and C are the values (±1 SD) of EP_0 and K_{Mg} as a function of ATP, respectively.

Table 2: Best Fitting Values of the Parameters of Eq 10 Adjusted to the Data in Figure 6

	8 μM [Mg]		1000 μM [Mg]	
parameter	10 μM [ATP]	1000 μM [ATP]	10 μM [ATP]	1000 μM [ATP]
EP_f (%)	75 ± 5	52 ± 5	67 ± 6	43 ± 7
kf (s^{-1})	0.65 ± 0.10	2.6 ± 0.6	1.3 ± 0.2	23 ± 8
EP_s (%)	25 ± 4	47 ± 5	33 ± 6	56 ± 6
ks (s^{-1})	0.014 ± 0.010	0.15 ± 0.03	0.033 ± 0.031	1.2 ± 0.2

of added Mg^{2+}. From the values in Table 2 and considering that the initial rate of dephosphorylation (r_0) can be calculated as

$$r_0 = EP_f k_f + EP_s k_s \qquad (11)$$

our results show that ATP produces only a 3-fold increase of the initial rate of dephosphorylation at 8 μM Mg^{2+} (from 49% to 142% per second) but a 12-fold increase at 1 mM Mg^{2+} (from 88% to 1056% per second). Note that ATP increases both the fast and slow dephosphorylation processes regardless of the Mg^{2+} concentration. It is generally accepted that the fast dephosphorylation component is due to that of E_2P while the slow component reflects the $E_1P \rightarrow E_2P$ transition (*5*). Therefore, an increase of the slow dephosphorylation component strongly suggests that this latter step is being accelerated by ATP.

At low ATP concentrations, Mg^{2+} does not produce any significant effect either on the dephosphorylation rate or on the proportion between EP_f and EP_s, suggesting that, at this concentration of ATP, Mg^{2+} does not affect the $E_1P \rightarrow E_2P$ conformational transition. In the presence of 1 mM ATP, Mg^{2+} accelerates both slow and fast dephosphorylation components, but in contrast with observations by Hersher et al. (*5*), it still does not show any significant effect on the proportion between EP_f and EP_s. This fact could be explained if the cation accelerated the $E_1P \leftrightarrow E_2P$ conformational transition similarly in both directions.

Interactions of Mg^{2+} and ATP with EP at 4 °C. A detailed study of the effect of Mg^{2+} on *E*P at different ATP concentrations was carried out. Figure 7 shows the results of experiments where *E*P was measured in steady-state conditions in media with 10 μM−2 mM ATP and from 8 to 500 μM Mg^{2+}. It can be seen that *E*P grows hyperbolically with [Mg^{2+}] for all ATP concentrations tested. The continuous lines represent the fitting of the following equation to the experimental data:

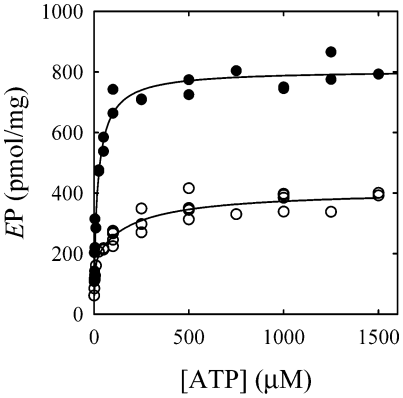

FIGURE 8: Phosphorylation of PMCA as a function of [ATP] at 25 °C. Phosphorylation was carried out in the presence of 8 μM (○) or 1 mM (●) Mg^{2+} ($n = 3$). The continuous lines represent the fitting of the sum of two Michaelis−Menten-like equations to the experimental data with best fitting parameters detailed in Table 3.

$$EP = EP_0 + \frac{(EP_{max} - EP_0)[Mg^{2+}]}{[Mg^{2+}] + K_{Mg}} \qquad (12)$$

where EP_0 and EP_{max} are the concentrations of *E*P in the absence of Mg^{2+} and at concentrations of the cation tending to infinity, respectively, and K_{Mg} is the concentration of Mg^{2+} for half-maximal activation.

Figure 7B shows the values of EP_0 and of EP_{max} as a function of [ATP], which are very similar to the results shown in Figure 2 for 8 μM and 1 mM Mg^{2+}, respectively. In Figure 7C we plotted the values of K_{Mg} as a function of [ATP]. Despite their large error, the values show a clear trend in the direction of ATP increasing the affinity for Mg^{2+}, as would be expected from the fact that Mg^{2+} seems to increase the affinity for ATP of the low-affinity component of the curves in Figure 2.

Effects of ATP on k_{pEP} at 25 °C. Reaction Scheme 1 has been formulated by combining the knowledge on the elementary steps and steady-state kinetics of the Ca^{2+}-ATPase (see page 114 in ref *2*), generally based on measurements carried out at different temperatures. In the case of P-ATPases, Arrhenius plots have been found to be nonlinear (*37*−*39*), showing higher slopes at lower temperatures. This deviation from linearity might mean that different steps during the reaction cycle become rate-limiting at different temperatures (*40*). One reason for the disagreement between our results and the predictions of Scheme 1 (e.g., for *E*P and k_{pEP}) could be that the experiments were done at low temperature. To investigate this hypothesis, we performed experiments and determined k_{pEP} at 25 °C using the same procedures described above for the experiments done at 4 °C.

Results of *E*P vs [ATP] measured at 25 °C are shown in Figure 8. We found that results are best described by a sum of two Michaelis−Menten-like equations. The best fitting values of the parameters are shown in Table 3. It seems interesting to note that, as we observed at 4 °C, Mg^{2+}

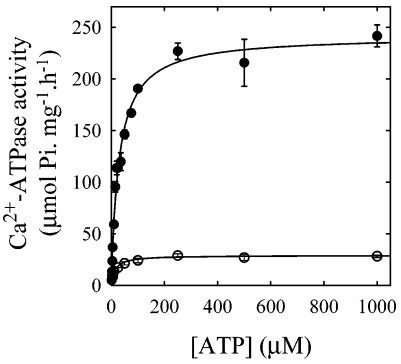

FIGURE 9: Ca^{2+}-ATPase activity as a function of [ATP] at 25 °C. Ca^{2+}-ATPase activity was measured in the same conditions as those used to measure *E*P in the presence of 8 μM (○) and 1 mM (●) Mg^{2+}. The continuous lines represent the fitting of a Michaelis−Menten equation to the experimental data.

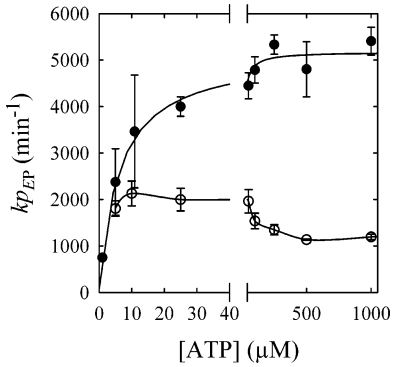

FIGURE 10: k_{pEP} as a function of [ATP] at 25 °C. Turnover of the phosphorylated intermediates of the erythrocyte PMCA was calculated as the ratio between *E*P (Figure 8) and Ca^{2+}-ATPase activity (Figure 9) in the presence of 8 μM (○) and 1 mM (●) Mg^{2+}. Values obtained were plotted as a function of ATP concentration. The continuous line represents the fitting of eq 6 to the experimental data obtained at 1 mM Mg^{2+} and drawn by eye for those obtained at 8 μM Mg^{2+}.

Table 3: Best Fitting Values of the Parameters of Eq 2 (Fixing $n = 1$) Adjusted to the Data in Figure 8

parameter	8 μM [Mg^{2+}]	1000 μM [Mg^{2+}]
K_{m1} (μM)	2.2 ± 1.2	0.9 ± 1.2
EP_{max1} (pmol/mg)	182 ± 34	176 ± 95
K_{m2} (μM)	228 ± 27	29 ± 9
EP_{max2} (pmol/mg)	193 ± 100	629 ± 92

increases the apparent affinity for ATP. However, in contrast with the results obtained at low temperature, the maximal *E*P level attained at 1 mM Mg^{2+} almost doubles that obtained at 8 μM Mg^{2+}.

Ca^{2+}-ATPase activity exhibits Michaelis−Menten kinetics (Figure 9). In agreement with previous results (*3*), Mg^{2+} does not modify considerably the apparent affinity for ATP (K_m values were respectively 14.3 ± 2.1 and 29.3 ± 2.4 μM at 8 μM and 1 mM [Mg^{2+}]). On the other hand, V_{max} increases from 29 ± 1 μmol/(mg·h) to 241 ± 6 μmol/(mg·h) when Mg^{2+} concentration rises from 8 μM to 1 mM.

We calculated k_{pEP} and plotted it as a function of [ATP] in Figure 10. At 1 mM Mg^{2+}, *E*P turnover increases with [ATP] from 80 ± 37 min^{-1} to 5094 ± 359 min^{-1} along a hyperbolic curve with $K_{0.5} = 6.3 \pm 1.4$ μM. Conversely, and as we observed at 4 °C, at 8 μM Mg^{2+} k_{pEP} grows to a maximum and then drops with increasing ATP concentration. Consequently, the same conclusions as those reached for the results obtained at 4 °C apply to the results at 25 °C.

Concluding Remarks. Results in this paper show (to our knowledge for the first time) that the steady-state level of *E*P varies with [ATP] in a nonhyperbolic manner when the concentration range of the nucleotide is extended to physiological levels. This complex behavior of phosphorylated intermediates is not observed for the results of the Ca^{2+}-ATPase activity. The fact that the K_m values for the activity are intermediate between those calculated for phosphorylation could be reflecting that the complex behavior observed for steady-state *E*P is hidden under the appearance of a single Michaelis−Menten curve for the activity.

Mg^{2+} seems to increase the apparent affinity for ATP of the low-affinity component of the steady-state level of *E*P, but it shows no significant effect on its high-affinity component or on the Ca^{2+}-ATPase activity.

The maximal steady-state level of *E*P never surpasses 50% of that obtained in the presence of saturating [La^{3+}], which is generally assumed to represent the total amount of active enzyme. This could indicate that dephosphorylation of E_2P is not the only rate-limiting step in the reaction cycle. In fact, Adamo et al. (*41*) observed that, for PMCA from pig red cells and working at 37 °C, the $E_2 \rightarrow E_1$ conformational transition should be at least one of the rate-limiting steps of the cycle. Alternatively, according to the proposal by Mahaney et al. for the SERCA (*42*), this result could be interpreted as if, in the absence of La^{3+}, two ATPase units were functioning in an out-of-phase mode, being only one of such units able to undergo phosphorylation at a time. If this were the case, studies involving chemical cross-linkers and fluorescence energy transfer (FRET) measurements would help to investigate a possible oligomeric organization of the ATPase in our preparation. We are at present carrying out FRET experiments with this aim.

The analysis of k_{pEP} shows that the currently accepted model fails to explain the kinetics of purified PMCA at physiological ATP concentrations. Whether a modified version of this model is able to explain the results or an entirely new model is necessary is being evaluated (unpublished results).

ACKNOWLEDGMENT

The authors are indebted to Professor Patricio J. Garrahan for helpful comments on the manuscript.

REFERENCES

1. Knauf, P. A., Proverbio, F., and Hoffman, J. F. (1974) Electrophoretic separation of different phosphoproteins associated with Ca-ATPase and Na, K-ATPase in human red cell ghosts, *J. Gen. Physiol. 63*, 324−336.
2. Rega, A. F., and Garrahan, P. J. (1986) *The Calcium Pump of Plasma Membrane*, CRC Press, Boca Raton, FL.
3. Richards, D. E., Rega, A. F., and Garrahan, P. J. (1978) Two classes of site for ATP in the Ca^{2+}-ATPase from human red cell membranes, *Biochim. Biophys. Acta 511*, 194−201.
4. Adamo, H. P., Rega, A. F., and Garrahan, P. J. (1990) Magnesium-ions accelerate the formation of the phosphoenzyme of the (Ca^{2+} + Mg^{2+})-activated ATPase from plasma membranes by acting on the phosphorylation reaction, *Biochem. Biophys. Res. Commun. 169*, 700−705.
5. Herscher, C. J., Rega, A. F., and Garrahan, P. J. (1994) The dephosphorylation reaction of the Ca^{2+}-ATPase from plasma membranes, *J. Biol. Chem. 269*, 10400−10406.

6. Garrahan, P. J., Rega, A. F., and Alonso, G. L. (1976) The interaction of magnesium ions with the calcium pump of sarcoplasmic reticulum, *Biochim. Biophys. Acta 448*, 121−132.
7. Caride, A. J., Rega, A. F., and Garrahan, P. J. (1986) The reaction of Mg^{2+} with the Ca^{2+}-ATPase from human red cell membranes and its modification by Ca^{2+}, *Biochim. Biophys. Acta 863*, 165−177.
8. Katz, S., and Blostein, R. (1975) Ca^{2+}-stimulated membrane phosphorylation and ATPase activity of the human erythrocyte, *Biochim. Biophys. Acta 389*, 314−324.
9. Chiesi, M., Zurini, M., and Carafoli, E. (1984) ATP synthesis catalyzed by the purified erythrocyte Ca-ATPase in the absence of calcium gradients, *Biochemistry 23*, 2595−2600.
10. Lichtner, R., and Wolf, H. U. (1980) Phosphorylation of the isolated high-affinity (Ca^{2+} + Mg^{2+}) ATPase of the human erythrocyte membrane, *Biochim. Biophys. Acta 598*, 472−485.
11. Sarkadi, B., Enyedi, A., Foldes-Papp, Z., and Gardos, G. (1986) Molecular characterization of the in situ red cell membrane calcium pump by limited proteolysis, *J. Biol. Chem. 261*, 9552−9557.
12. Rega, A. F., and Garrahan, P. J. (1975) Calcium ion-dependent phosphorylation of human erythrocyte membranes, *J. Membr. Biol. 22*, 313−327.
13. Graf, E., Verma, A. K., Gorski, J. P., Lopaschuk, G., Niggli, V., Zurini, M., Carafoli, E., and Penniston, J. T. (1982) Molecular properties of calcium-pumping ATPase from human erythrocytes, *Biochemistry 21*, 4511−4516.
14. Kosk-Kosicka, D., Scaillet, S., and Inesi, G. (1986) The partial reactions in the catalytic cycle of the calcium-dependent adenosine triphosphatase purified from erythrocyte membranes, *J. Biol. Chem. 261*, 3333−3338.
15. Garrahan, P. J., and Glynn, I. M. (1967) The incorporation of inorganic phosphate into adenosine triphosphate by reversal of the sodium pump, *J. Physiol. (London) 192*, 237−256.
16. Echarte, M. M., Levi, V., Villamil, A. M., Rossi, R. C., and Rossi, J. P. (2001) Quantitation of plasma membrane calcium pump phosphorylated intermediates by electrophoresis, *Anal. Biochem. 289*, 267−273.
17. Niggli, V., Penniston, J. T., and Carafoli, E. (1979) Purification of the (Ca^{2+}-Mg^{2+})-ATPase from human erythrocyte membranes using a calmodulin affinity column, *J. Biol. Chem. 254*, 9955−9958.
18. Gietzen, K., Konrad, R., Tejcka, M., Fleischer, S., and Wolf, H. U. (1981) Purification, characterization, and reconstitution of the Ca^{2+}-transport system (high-affinity Ca^{2+}, Mg^{2+}-ATPase) of the human erythrocyte membrane, *Acta Biol. Med. Ger. 40*, 443−456.
19. Castello, P. R., Gonzalez, Flecha, F. L., Caride, A. J., Fernandez, H. N., Delfino, J. M., and Rossi, J. P. (1997) The membrane topology of the amino-terminal domain of the red cell calcium pump, *Protein Sci. 6*, 1708−1717.
20. Peterson, G. L. (1977) A simplification of the protein assay method of Lowry et al. which is more generally applicable, *Anal. Biochem. 83*, 346−356.
21. Kratje, R. B., Garrahan, P. J., and Rega, A. F. (1983) The effects of alkali metal ions on active Ca^{2+} transport in reconstituted ghosts from human red cells, *Biochim. Biophys. Acta 731*, 40−46.
22. Schwarzbaum, P. J., Kaufman, S. B., Rossi, R. C., and Garrahan, P. J. (1995) An unexpected effect of ATP on the ratio between activity and phosphoenzyme level of Na^+/K^+-ATPase in steady state, *Biochim. Biophys. Acta 1233*, 33−40.
23. Akaike, H. (1973) A new look at the statistical model identification, *IEEE Transactions on Autom. Control 19*, 716−723.
24. Muallem, S., and Karlish, S. J. (1983) Catalytic and regulatory ATP-binding sites of the red cell Ca^{2+} pump studied by irreversible modification with fluorescein isothiocyanate, *J. Biol. Chem. 258*, 169−175.
25. Wong, J. T.-F. (1975) *Kinetics of Enzyme Mechanisms*, p 75 ff, Academic Press, London.
26. Muallem, S., and Karlish, S. J. (1980) Regulatory interaction between calmodulin and ATP on the red cell Ca^{2+} pump, *Biochim. Biophys. Acta 597*, 631−636.
27. Muallem, S., and Karlish, S. J. (1981) Studies on the mechanism of regulation of the red-cell Ca^{2+} pump by calmodulin and ATP, *Biochim. Biophys. Acta 647*, 73−86.
28. Rossi, J. P., Rega, A. F., and Garrahan, P. J. (1985) Compound 48/80 and calmodulin modify the interaction of ATP with the (Ca^{2+} + Mg^{2+})-ATPase of red cell membranes, *Biochim. Biophys. Acta 816*, 379−386.
29. Stieger, J., and Luterbacher, S. (1981) Some properties of the purified (Ca^{2+} + Mg^{2+})-ATPase from human red cell membranes, *Biochim. Biophys. Acta 641*, 270−275.
30. Schatzmann, H. J., and Burgin, H. (1978) Calcium in human red blood cells, *Ann. N.Y. Acad. Sci. 307*, 125−147.
31. Szasz, I., Sarkadi, B., Schubert, A., and Gardos, G. (1978) Effects of lanthanum on calcium-dependent phenomena in human red cells, *Biochim. Biophys. Acta 512*, 331−340.
32. Luterbacher, S., and Schatzmann, H. J. (1983) The site of action of La^{3+} in the reaction cycle of the human red cell membrane Ca^{2+}-pump ATPase, *Experientia 39*, 311−312.
33. Barrabin, H., Scofano, H. M., and Inesi, G. (1984) Adenosinetriphosphatase site stoichiometry in sarcoplasmic reticulum vesicles and purified enzyme, *Biochemistry 23*, 1542−1548.
34. Jørgensen, P. L. (1988) *Methods Enzymol. 156*, 29−43.
35. Garrahan, P. J., and Rega, A. F. (1978) Activation of partial reactions of the Ca^{2+}-ATPase from human red cells by Mg^{2+} and ATP, *Biochim. Biophys. Acta 513*, 59−65.
36. Rega, A. F., and Garrahan, P. J. (1978) Calcium ion-dependent dephosphorylation of the Ca^{2+}-ATPase of human red-cells by ADP, *Biochim. Biophys. Acta 507*, 182−184.
37. Inesi, G., Millman, M., and Eletr, S. (1973) Temperature-induced transitions of function and structure in sarcoplasmic reticulum membranes, *J. Mol. Biol. 81*, 483−504.
38. Lee, A. G., Birdsall, N. J., Metcalfe, J. C., Toon, P. A., and Warren, G. B. (1974) Clusters in lipid bilayers and the interpretation of thermal effects in biological membranes, *Biochemistry 13*, 3699−3705.
39. Dean, W. L., and Tanford, C. (1978) Properties of a delipidated, detergent-activated Ca^{2+}-ATPase, *Biochemistry 17*, 1683−1690.
40. I. H. S. (1975) *Enzyme Kinetics*, p 934, John Wiley & Sons, New York.
41. Adamo, H. P., Rega, A. F., and Garrahan, P. J. (1990) The E2 in equilibrium E1 transition of the Ca^{2+}-ATPase from plasma membranes studied by phosphorylation, *J. Biol. Chem. 265*, 3789−3792.
42. Mahaney, J. E., Thomas, D. D., and Froehlich, J. P. (2004) The time-dependent distribution of phosphorylated intermediates in native sarcoplasmic reticulum Ca^{2+}-ATPase from skeletal muscle is not compatible with a linear kinetic model, *Biochemistry 43*, 4400−4416.

BI061857X